Engineering Structures 179 (2019) 211–224

Contents lists available at ScienceDirect

Engineering Structures

journal homepage: www.elsevier.com/locate/engstruct

Blast resistance of externally prestressed RC Beam: A theoretical approach

Yi Fan[a], Li Chen[a,b,*], Qin Fang[a], Tengfei Wang[a]

[a] State Key Laboratory of Disaster Prevention & Mitigation of Explosion & Impact, Army Engineering University of PLA, Nanjing, Jiangsu 210007, China
[b] School of Civil Engineering, Southeast University, Nanjing, Jiangsu 210096, China

ARTICLE INFO

Keywords:
Externally prestressed beam
Blast loading
Rate-sensitive model
Dynamic response
Layered-section method

ABSTRACT

Externally prestressed reinforced concrete (EPC) is employed in long-span civil infrastructure, and a simplified dynamic analytical method is required to evaluate the blast-resistant performance of these EPC components. A theoretical approach is proposed that combines the elasto-viscoplastic rate-sensitive model with an improved layered-section method to predict the dynamic responses of EPC beams subjected to blast loadings, based on an equivalent single-degree-of-freedom system. A corresponding calculation program is compiled on the MATLAB platform. The proposed approach and the compiled program are validated by application to existing static and blast testing data, as well as the corresponding finite element calculation results. Three key parameters—the conventional reinforcement ratio ρ_s, the prestressing reinforcement ratio ρ_p, and the span-depth ratio l/h—that significantly affecting the dynamic responses of the EPC beam to explosion are discussed, providing useful design insights. The analytical results indicate that the determination of the three affecting parameters should be balanced to achieve a higher blast resistance in designing the EPC beam.

1. Introduction

External prestressing is a technique in which concrete structural members are prestressed longitudinally using tendons located entirely outside the concrete section. This technique is widely used to strengthen or rehabilitate existing concrete structures and in the construction of new concrete structures because of its superiority compared with other conventional prestressing techniques [1]. The advantages of external prestressing tendon systems include their easier tendon layout and placement, better corrosion protection, and significant contribution to restricting the deflection of long-span structures [2]. Furthermore, externally prestressed reinforced concrete (EPC) structures can potentially resist explosion, and are therefore used in key civil infrastructure, particularly in long-span concrete structures.

Because of the ubiquity and importance of the external prestressing technique, the associated static behaviors have been intensively studied, including in engineering applications. The use of external prestressed tendons increases the load-carrying performance of beam components, which has been confirmed both theoretically and experimentally [3–7]. The load-bearing capacity is influenced by several factors, researchers have paid much attention to study the effects of these factors. Aparicio et al. [8] tested five monolithic and three segmental EPC beams in bending failure and in combined bending and shear failure. They observed that reducing the length of the tendon will increase the ultimate load-bearing capacity. Lou et al. [9] and El-Ariss [10] studied the flexural behavior of EPC beams, the results showed that high span-to-depth ratios led to a significant decrease in the eccentricity and therefore resulted in reduced rigidity and lower flexural capacity. The setting of the external tendons has a great influence on the load-bearing capacity of structures. Ghallab and Beeby [11] found that the ultimate stress in the external tendon was slightly affected by the internal bonded steel ratio, and was significantly affected by the value of the prestress, the number of deviators, the concrete strength, and the ratio of the distance between deviators to the span. Cao et al. [12] investigated the design of anchor blocks for external tendons experimentally, and found that large shear span-depth ratio decreased the ultimate loads of anchor block specimens. Ghallab [13] presented a simple method of calculating the increase in stress in external prestressing tendons at the ultimate stage and verified this method in relation to experimental results: the calculation could be applied at any loading stage and could used without any limitation on the number of deviators, loading pattern, deviated tendon profile, eccentricity of the external tendons, or span/depth ratio. In addition, the method could be used for both steel and/or fiber reinforced polymer tendons. Pisani [14]

Abbreviations: EPC, externally prestressed reinforced concrete; FE, finite element; RC, reinforced concrete; SDOF, single-degree-of-freedom

* Corresponding author at: State Key Laboratory of Disaster Prevention & Mitigation of Explosion & Impact, Army Engineering University of PLA, Nanjing, Jiangsu 210007, China.
E-mail address: chenli1360@qq.com (L. Chen).

https://doi.org/10.1016/j.engstruct.2018.10.079
Received 21 March 2018; Received in revised form 25 September 2018; Accepted 29 October 2018

introduced two numerical methods that was able to describe the time evolution of both the stress distribution and the displacement of a simply supported EPC beam under long-term loading: one method offered a solution that was theoretically exact and mathematically almost exact; the other method significantly simplified the computation and was demonstrated to yield a solution that was sufficiently refined to be acceptable in common practice.

In addition, shear behaviors and moment redistributions have also been investigated in extant researches. Qi et al. [15] investigated the shear behavior and ultimate capacity of nine reinforced concrete (RC) beams prestressed with external tendons, and the test results showed that the presence of external prestressing enhanced the shear cracking load and shear strength by 150% and 56%, respectively. El-Shafiey and Atta [16] also found external prestressing to be a highly effective strengthening method that increased the shear load-carrying capacity of existing concrete beams. Wang et al. [17] presented a model to predict the shear strength and possible modes of failure of EPC beams and generate optimal strut-and-tie models for the design of complex EPC members, and then derived a theoretical formula of the shear strength; their calculated results agreed well with the experimental data. Song et al. [18] studied the moment redistribution in EPC continuous curved beams using three specimens with different curvature radii, and they demonstrated that the results obtained using the current design codes yielded conservative predictions of the moment redistribution. Lou et al. [19] numerically studied the flexural responses of two-span continuous EPC beams having various linearly-transformed cable profiles, and they found that the redistribution of the moment over the center support was significantly affected by the linear transformation of the cable line.

Inconsistencies with regard to ductility findings have also been reported in extant studies. Grace and AbdeiSayed [20] examined the responses of four bridge models with unbonded externally draped carbon fiber reinforced polymer tendons under static and repeated loads. They concluded that the use of such tendons improved ductility. An experimental study of EPC beams was conducted by Ghallab [21], and the test results showed a significant reduction in the ductility of the beams. Although the research on the static behaviors of EPC structures is comprehensive, more investigations are needed because of the complications resulting from diverse influencing factors and potential conflicts among them.

Very limited studies concerning the blast-resistant performance of prestressed RC structures were found in the open literature, and the prestressing tendons of these structures are all inside the structural members. Chen et al. [22] proposed an analytical method to investigate the dynamic responses of partially prestressed RC beams subjected to blast loadings, and found that the dynamic resistance improved with increased initial prestressing force and partial prestressing ratio. Chen et al. [23] studied the dynamic response of a simply supported prestressed RC beam under blast loadings by using finite element (FE) code in LS-DYNA, and they found that optimal prestressing levels and higher concrete compressive strength were necessary to enhance the blast loading capacities of RC beams. Ngo et al. [24] investigated the blast resistance of three partially prestressed panels made of ultra-high strength concrete, and the three panels were able to sustain considerable deflections with only minor cracks. Cramsey and Natio [25] tested a 30-ft partially prestressed concrete panel subjected to different blast loadings, and found that the panel could rotate 2.7° without failure under the highest-magnitude blast loading. Cofer et al. [26] created a FE model of a precast, prestressed concrete girder subjected to near field blast loading above and below, and verified the model by full-scale experiments. The primary mode of failure for both scenarios was dominated by the concrete smash and shear failure, leading to overall structural instability and collapse.

Park et al. [27] examined the behavior of a bridge strengthened by externally prestressed tendons under a live-truck load. The results indicated that the strengthening had little effect on the natural frequency and the shape of the bridge. However, the strengthening reduced the mid-span deflection by 10–24% and increased the live load carrying capacity. Chen et al. [28] studied the vibration performance of a long-span concrete floor during the structure's daily use and under controlled human activities using a unique external prestressing system, and compared the structure's performance with the design guidelines, concluding that a vibration amplitude threshold was more suitable for assessing the vibration serviceability than a vibration frequency threshold. Miyamoto et al. [29] studied the effects of external prestressing on the flexural vibration characteristics of a composite girder and proposed a formula to calculate the natural frequency. Analytical and experimental results showed that with a slightly eccentric tendon arrangement, the natural frequency decreased as the amount of prestressing force increased, whereas the natural frequency increased as the amount of prestressing force increased with the more eccentric tendon arrangement. An analytical model of an EPC beam was established by Shi et al. [30], in which the prestressing force was identified by combining the frequency equation and the measured frequencies, and the prestress force thus identified was in good agreement with the test results.

As shown in the above literature review, existing investigations on the external prestressing technique are mainly focusing on the flexural behaviors and vibration performance under ultimate loads, service loads, and fatigue loads, and unfortunately, studies on the blast-resistant capacities of EPC structures are very limited.

Prestressed structures were initially considered to have lacked ductility and not be suitable for use in blast-resistant structures [22]. Additionally, a methodology specific to the design of prestressed structures subjected to blast loadings has been lacking in existing protective-design manuals. However, with the recent development in prestressing technology and research, it has been demonstrated that partially prestressed RC beams with a reasonable design possess has good ductility when subjected to blast loadings [22,31]. The prestressed tendons of the partially prestressed structures are inside, while the prestressed tendons of the EPC structures are arranged outside the concrete body. The only connection points between a prestressed tendon and an EPC structure are located at the deviator and anchorage, and a possible connection failure may lead to unknown, more severe damage. Therefore, theoretical and experimental studies of EPC structures under blast loading is of interest for long-span structural components. However, existing theoretical methods for analysis of EPC structures are not applicable to structures subjected to blast loadings with extremely short duration. This is because the effect of the strain rate on material behaviors and the effect of the inertia forces (mass × acceleration) must be considered during dynamic analysis of protective structures [32].

Therefore, this study provides a simple and effective method for predicting the dynamic flexural responses of EPCs subjected to uniformly distributed blast loadings by combining a rate-sensitive material model and an improved layered section method, assuming the deformation mode of the EPC beams is flexural only or flexural governed. The accuracy and applicability of the proposed method were verified by FE calculation and existing experimental data. Key parameters were identified, providing useful design insights for engineering applications.

2. Dynamic resistance model

The proposed approach was developed for an EPC beam that has a pair of draped tendons and a corresponding deviator on the soffit at mid-span of the beam. A schematic diagram of a simply supported EPC beam is shown in Fig. 1(a), the beam is subjected to a uniformly distributed blast loading. The force analysis model of the EPC beam is shown in Fig. 1(b), where the prestressing force P is treated as external loads [33], θ is the tendon angle, e is the eccentricity and δ denotes the deflection at mid-span.

As shown in Fig. 1(b), the external prestressing effect of the steel

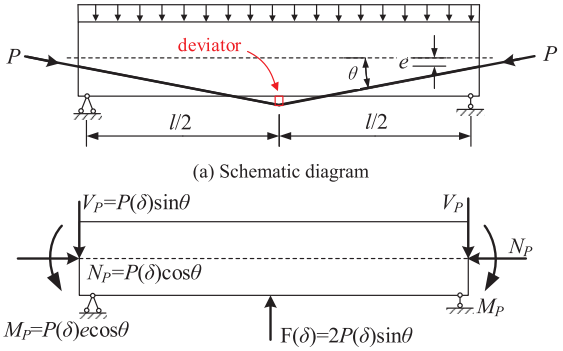

Fig. 1. Analytical model of a simply supported EPC beam. ***l***: span length, ***P(δ)***: prestressing force, and ***F(δ)***: vertical restoring force. (b) Force analysis model.

tendon was decomposed to external vertical force $V_P = P(\delta)\sin\theta$ at the end; external axial force $N_P = P(\delta)\cos\theta$; external bending moment $M_P = P(\delta)e\cos\theta$; and external restoring force $F(\delta) = 2P\sin\theta$ at mid-span.

2.1. Stress-strain relation of concrete and steel

The dynamic responses of RC components under external loads depends to a large extent on the stress-strain relation of concrete and steel material. A simplified stress-strain envelope with an unloading-reloading path for the concrete material, introduced by Izzuddin and Fang [34], was adopted in this study, as illustrated in Fig. 2. There are three discrete regions in the monotonic concrete stress-strain relations:

$$\begin{cases} \sigma = \frac{f_c}{\varepsilon_0}\varepsilon & 0 \le \varepsilon \le \varepsilon_0 \\ \sigma = f_c[1 - Z(\varepsilon - \varepsilon_0)] & \varepsilon_0 \le \varepsilon \le \varepsilon_{40c} \\ \sigma = 0.4 f_c & \varepsilon_{40c} \le \varepsilon \le \varepsilon_u \end{cases} \quad (1)$$

in which

$$Z = \frac{0.5}{\frac{3 + 0.29 f_c}{145 f_c - 1000} - \varepsilon_0}, \quad \varepsilon_0 = (1.35 + 0.02 f_c) \times 10^{-3}$$

f_c and ε_0 are the compressive strength and corresponding critical strain to peak stress, respectively; ε_{40c} and ε_u represent the strain corresponding to the residual strength of $0.4f_c$ and the ultimate strain, respectively; and f_t is the tensile strength. The computational analysis of RC structures subjected to dynamic loadings requires stress–strain models to reproduce the dynamic behaviors of the structure. It is well known that 'under cyclic or dynamic loads, concrete may experience complex loading processes involving not only full unloading–reloading cycles in compression or tension, but also partial unloading and reloading processes and mixed cycles involving compression and tension stresses and cracking' [35]. The blast loading can be considered as a monolithic load, however, it usually induces forced vibration and free vibration of RC structures depending on the loading duration and inherent frequency. The unloading-reloading branches are defined to simulate the vibration behaviors of concrete under or after blast loadings. Therefore, simplified unloading-reloading curves are generally adopted for their simplicity and computational efficiency in providing theoretical analysis of concrete structures, which is shown in Fig. 2.

The stress-strain relation of conventional steel material is considered as multi-linear in both tension and compression. The longitudinal stirrup steel bar and prestressed steel tendon are typically modeled as linear elastic, linear strain-hardening materials in this study. Therefore, the following stress-strain relation, which was introduced by [34], was adopted to describe the monotonic envelope of the conventional steel bar and prestressed steel tendon, as shown in Eqs. (2) and (3), respectively. The unloading-reloading curves of the steel reinforcement are also defined with the similar reason to concrete, as shown in Fig. 3. The unloading and reloading stiffness was assumed to be the same as the initial stiffness for simplicity and computational efficiency [22].

For conventional steel bars,

$$\begin{cases} \sigma_s = E_s\varepsilon & 0 \le \varepsilon \le \varepsilon_s \\ \sigma_s = f_s + E_{sp}(\varepsilon - \varepsilon_s) & \varepsilon_s \le \varepsilon \end{cases} \quad (2)$$

For the prestressed steel tendon,

$$\begin{cases} \sigma_p = E_p\varepsilon & 0 \le \varepsilon \le \varepsilon_y \\ \sigma_p = f_y + E_{pu}(\varepsilon - \varepsilon_y) & \varepsilon_y \le \varepsilon \end{cases} \quad (3)$$

where $\sigma_s(\sigma_p)$ and ε are the stress and strain of a conventional steel bar (prestressed steel tendon), respectively; $f_s(f_y)$ and $\varepsilon_s(\varepsilon_y)$ are the yield stress and corresponding yield strain of a conventional steel bar (prestressed steel tendon), respectively; $f_u(f_{pu})$ and $\varepsilon_u(\varepsilon_{pu})$ are the ultimate stress and corresponding ultimate strain of a conventional steel bar (prestressed steel tendon), respectively; and $E_s(E_p)$ and $E_{sp}(E_{pu})$ are the elastic modulus and corresponding hardening modulus of a conventional steel bar (prestressed steel tendon), respectively.

2.2. Rate-sensitive material model

Concrete and steel are both strain-rate dependent materials, and high strain rate tend to enhance their respective strengths. The quasi-static strain rate generally lies in the range of 10^{-6}–$10^{-4}\,s^{-1}$, however, the strain rate induced by the blast loading in the concrete structures can be as high as 10^{1}–$10^{3}\,s^{-1}$. Consequently, effects of the strain rate on material behavior must be considered in the investigation of engineering structures subjected to severe dynamic loadings, including blast loadings and impact loadings [36,37]. If no strain rate analyses are to be performed, it is recommended that the dynamic yield strength of steel and concrete be 10% and 20% greater, respectively, compared to the static yield strength [38], these are correspond to average increases in yield strength. In fact, the local strain rate along the beam is different

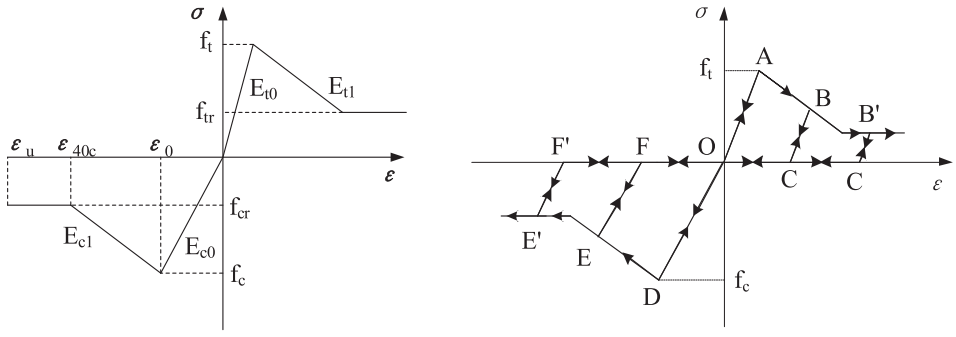

Fig. 2. Stress-strain relation with unloading-reloading path of concrete (the ordinate representing tensile strength of concrete has been enlarged for clarity).

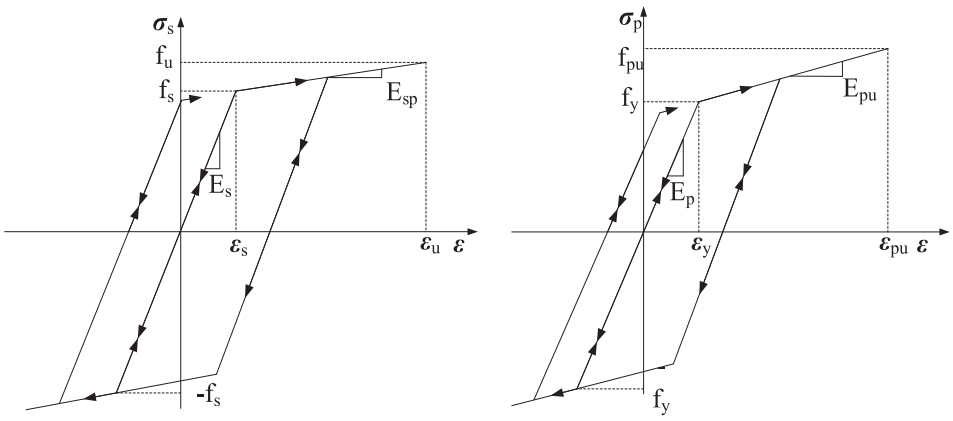

(a) Conventional steel bar (b) Prestressed steel tendon

Fig. 3. Stress-strain curve with unloading-reloading path of steel bar and tendon. (a) Conventional steel bar. (b) Prestressed steel tendon.

at different locations and is a function of time. However, constant enhancement factors for steel and concrete are not sufficiently accurate during dynamic-response analysis of EPC beams subjected to blast loadings. An improved elasto-viscoplastic rate-sensitive model has, therefore, been employed to accurately account for the strain-rate effect on steel and concrete materials. A detailed description of the said model can be found in [34] and [39].

Among the current mathematical models used in structural analysis, the elasto-viscoplastic rate-sensitive model proposed by Malvern [40] and Perzyna [41] has been widely applied to consider the effects of the strain rate, which has been used and described in detail in [22]. According to Perzyna, the response of an elasto-viscoplastic material comprises an elastic component, which develops instantaneously, and a time-dependent viscoplastic component, which is related to the overstress. As presented in Eq. (4), the parameter X represents the overstress, namely, the difference between the dynamic stress and the corresponding static stress:

$$X = \sigma - g(\varepsilon) \tag{4}$$

where σ is the dynamic stress, and $g(\varepsilon)$ represents the static stress in the plastic range. Stresses generated under quasi-static loading and blast loading correspond to static and dynamic stresses, respectively.

The following three-parameter relationship between the overstress X and strain-rate $\dot{\varepsilon}$ was derived [34] and employed in this study:

$$X = F(\dot{\varepsilon}) = SN\ln\left(1 + \left(\frac{\dot{\varepsilon}}{\dot{\varepsilon}_*}\right)^{1/N}\right) \tag{5}$$

As presented in Eq. (6), the function $f(X)$ is the strain-rate function, and $f(X)$ can be expressed as

$$f(X) = E(1-\mu)\dot{\varepsilon}_*\left[\exp\left(\frac{X}{SN}\right) - 1\right]^N \tag{6}$$

where $\dot{\varepsilon}_*$, S, and N are the model parameters, which can be determined by tests of constant strain rate. The model parameters provide more flexibility in fitting experimental data over a wider range of strain rate, and thus the model can be applied to concrete, steel, and other materials. The parameters used in the rate-sensitive model are listed in Section 4.2.1.

2.3. Model of resistance to external dynamic load

This section presents a resistance model for analyzing the dynamic responses of EPC beams under blast loadings. First, the relationship between the mid-span deflection δ and section curvature φ is obtained by the plastic hinge assumption. Second, the improved layered section method is used to calculate the bending moment M corresponding to different curvatures φ of the beam section, and then the relationship between the bending moment M and curvature φ is obtained. Third, the dynamic resistance R of the beam is calculated based on the bending moment M considering strain-rate effects. The relationship between the mid-span deflection δ and the strain of the external prestressing tendons ε_p can be calculated through their geometric relations. Fig. 4 summarizes these calculation steps, which are detailed in the following subsections.

The proposed dynamic resistance model is based on the following assumptions:

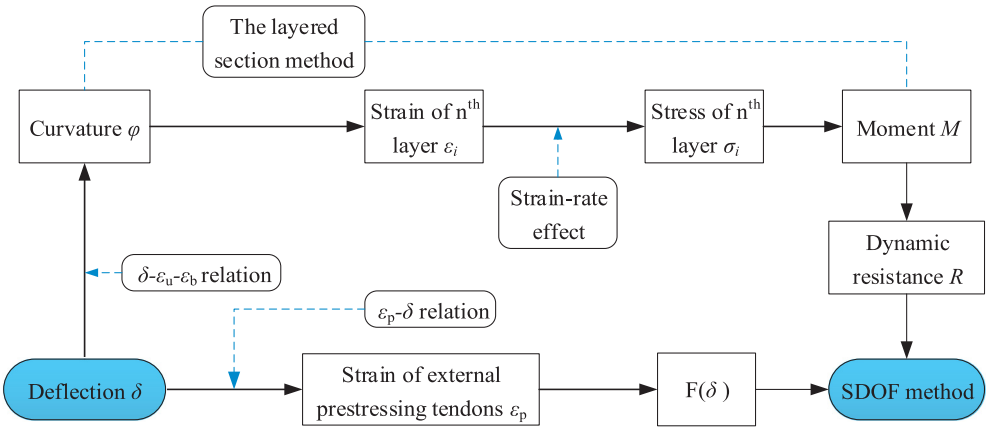

Fig. 4. Sketch of the dynamic resistance model.

(1) Boundary slip between concrete and steel bars is not considered, and the section is assumed to remain planar after bending, modeled as a linear strain distribution.
(2) Only flexural deformation occurs during the loading process; shear deformation and shear failure are not considered in this study, because the SDOF approach has limitation that requires applicable shape function, such as the proposed approach is obviously not suitable to the case of shear failure.
(3) The portions of the tendons between the ends and the deviator at the mid-span are straight.
(4) The difference in the stress between the anchorage and prestressing ends due to possible friction at the deviator is negligible for the draped external tendon profile [2].

2.3.1. M-φ relation for the mid-span cross-section with external prestressing load

The relation between the section moment M and curvature φ of a simply supported EPC beam can be calculated by improving the layered section method, where the prestressing force of the tendon could be treated as external load, as presented in Fig. 1(b). The layered section method avoids numerical oscillations before section yielding and therefore enables efficient analysis of RC structures [42].

The strain and force distributions across a typical rectangular section of EPC beam are shown in Fig. 5, where the cross-section is divided into n layers, and layers $n + 1$ and $n + 2$ represent the conventional compressive steel bars and conventional tensile bars, respectively.

Then, the following steps can be taken to determine the M-φ relationship:

(1) Input the dimensions of the rectangular section, the eccentricity, the initial curvature φ, and the initial strain at mid-depth $\bar{\varepsilon}$, which are assumed to be 0 at the first step, i.e., $\varphi = 0$ and $\bar{\varepsilon} = 0$.

(2) Calculate the strain of each layer ε_i based on the plane section assumption, and then determine the material stress according to the stress-strain curves of concrete and steel:$\varepsilon_i = \bar{\varepsilon} - z_i\varphi$, where $z_i = -\frac{h}{2} + \frac{h(i-1)}{n} + \frac{h}{2n}$ is the distance from the center of the i^{th} layer to the middle axis.

(3) Change the value of $\bar{\varepsilon}$ until horizontal force equilibrium is reached.

$$\sum (N_{ci} + N_{ti} + N_{si}^{'} + N_{si}) = N \tag{7}$$

where N_{ci} and N_{ti} are the total compressive and tensile force of concrete in the i^{th} layer, respectively; N_{si} and $N_{si}^{'}$ are the total compressive and tensile force of the steel bars, respectively; and N is the external axial force, which is a function of $P(\delta)$, corresponding to φ ($P(\delta)$, as described in detail in Section 2.3.3).

(4) Output the cross-sectional moment M and corresponding curvature φ after equilibrium reached:

$$M = \sum (M_{ci} + M_{ti} + M_{si}^{'} + M_{si}) \tag{8}$$

where M_{ci} and M_{ti} are the moment of the concrete in the i^{th} layer to the middle axis; $M_{si}^{'}$ and M_{si} are the moment of the steel bars in the i^{th} layer to the middle axis; and M is the external moment applied on the cross-section.

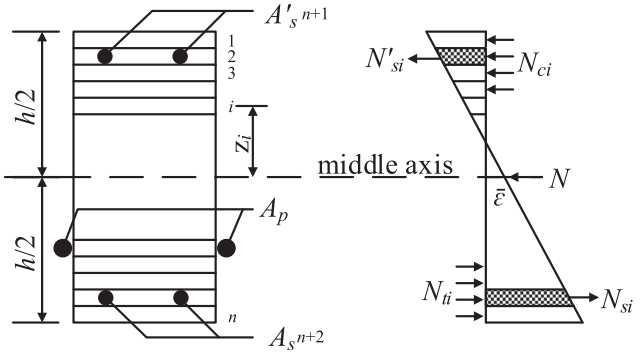

Fig. 5. Cross-section analysis.

(5) Increase the curvature by steps $\varphi = \varphi \pm \Delta\varphi$ and repeat steps (2) through (4). Store the results of M and φ at each step, where '–' represents a curvature that is increasingly negative.

The prescribed method of adjusting the strain $\bar{\varepsilon}$ at mid-depth of the cross-section is very critical. An extrapolation-based method was first adopted in this study to determine an appropriate value of $\bar{\varepsilon}$. However, the extrapolation process has a tendency fall into an "endless loop" once section yielding occurs. In this study, therefore, the extrapolation step was replaced by interpolation during the stage-softening stage, which would be obviously much easier to convergence, as reported by Pan et al. [43]. Detailed information regarding the layered-section method can be found in [43], which includes a flowchart for calculating the sectional moment-curvature curve. The difference between their procedure and the one followed in this study is that the influence of prestressing forces within external tendons is considered in the proposed study while that of temperature is not.

Computation of the M-φ relationship of the EPC beam is actually divided into two stages. The first stage applies the initial decomposed axial force and initial bending moment as external loads on the section of the beam, and obtains negative M_0 and φ_0 of the section in the initial state by decreasing φ, as shown in Fig. 1(b), which is caused by the external prestressing force. The second stage increases the curvature incrementally based on the stress state in the first period to obtain the M-φ relation of the cross-section.

2.3.2. Computation of the δ-ε_u-ε_b relation for the plastic hinge

A constitutive equation of the employed rate-sensitive material model with three parameters provides the relationship between overstress and strain rate. Hence, establishing the relation between the mid-span deflection δ and material strain is critical to establish the proposed model of resistance to external dynamic load, which depends on the rate-sensitive effects.

A large number of experimental results have shown that a plastic hinge appears in RC beams with large bending moments before the beams fail. There is no significant deformation or damage to the other portions of the beams, except in the plastic section. A similar phenomenon has been observed in experiments on EPC beams [2,44,45]. For the EPC beam with a deviator at the mid-span, the vertical force $F(\delta)$ provided by the deviator makes the maximum compressive stress of the concrete near the deviator more evenly distributed along the length of the beam, such that the length of the plastic hinge area is longer than that of a beams with no deviator [46,47].

Therefore, both sides of the plastic hinge can be assumed to be rigid after the plastic hinge forms in the simply supported EPC beam with a mid-span deviator. The beam can then be divided into three sections, as shown in Fig. 6.

Assuming that the length of the upper surface of the plastic hinge is $2s_u$ and the length of the bottom surface is $2s_b$, the compressive strain of the concrete material at the upper surface is $\varepsilon_u = \frac{s_u - Z}{Z}$ and the tension strain of the bottom surface is $\varepsilon_b = \frac{s_b - Z}{Z}$, where $2Z$ is the length of the plastic hinge. If the relations between δ and both ε_u and ε_b can be obtained, the relations between the mid-span deflection and the cross-sectional strains of different layers can also be established by linear - interpolation.

Investigators have not reached a consensus regarding an appropriate expression for the length of an equivalent plastic hinge because of the different important parameters that can be considered and the scattered test results, although extensive research has been performed on this topic [48,49]. The length of the plastic hinge can be estimated by the following modified expression to account for the effect of the prestressing force [50]:

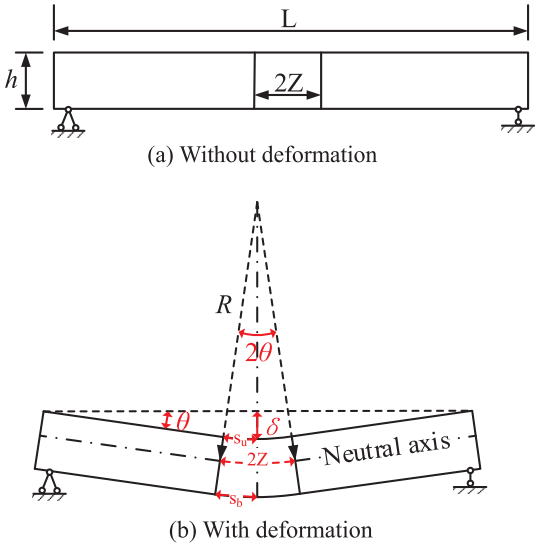

Fig. 6. Deformation diagram of a simply supported EPC beam. (a) Without deformation. (b) With deformation.

$$Z = \frac{1}{2}[0.5h_0 + 0.05a(1-\beta_p)] \tag{9}$$

where h_0 represents the effective depth of the beam; $\beta_p = \frac{A_p\sigma_{pe}}{f_c b h_0}$ is the index of the ratio of prestressing reinforcement; A_p is the area of the prestressing steel tendons; σ_{pe} is the initial stress of the prestressing tendons; b is the overall width of the cross-section; and a denotes the length of shear span.

The theoretical height of the compression zone (equivalent rectangular stress block) of the beam section is assumed to bex_c. According to the concrete structure design principle [51], the relative height of the compression zone of the beam section x can be described as follows:

$$\begin{cases} \alpha_1 f_c b x + f_y^{'} A_s^{'} = f_y A_s \\ \beta_1 = \frac{x}{x_c} \end{cases} \tag{10}$$

where A_s and f_y are the area and yield stress of sections of conventional tensile steel bars, respectively; $A_s^{'}$ and $f_y^{'}$ are the area and yield stress of sections of conventional compressive steel bars, respectively; and α_1 is the ratio of the stress value of the equivalent rectangular stress block to the compressive strength f_c of the concrete. The geometric relationship among the related parameters can then be described by the following equations, according to Fig. 6.

$$\begin{cases} \theta = \frac{Z}{R} = \frac{s_u}{R - x_c} = \frac{s_b}{R + h - x_c} \\ tan\theta = \frac{R - x_c - \frac{R - x_c - \delta}{\cos\theta}}{\frac{L}{2} - Z} \end{cases} \tag{11}$$

The relations between δ and ε_1 and ε_2 are established by combining Eqs. (10) and (11) as follows:

$$\begin{cases} \delta = cos\frac{Z\varepsilon_u}{x_c}\left[\frac{x_c}{\varepsilon_u} + x_c - \left(\frac{L}{2} - Z\right)\tan\frac{Z\varepsilon_u}{x_c}\right] - \frac{x_c}{\varepsilon_u} - x_c \\ \delta = cos\frac{Z\varepsilon_b}{x_c - h}\left[\frac{x_c - h}{\varepsilon_u} + x_c - \left(\frac{L}{2} - Z\right)\tan\frac{Z\varepsilon_b}{x_c - h}\right] - \frac{x_c - h}{\varepsilon_b} - x_c \end{cases} \tag{12}$$

The definitions of certain parameters are shown in Fig. 6. The strain of the n^{th} layerε_n of the mid-span section can be obtained via the linear interpolation method according to the plane section assumption.

2.3.3. Computation of the ε_p-δ relation for the external prestressing tendon

Many equations have been proposed to express the stress in externally prestressed tendons. Unfortunately, despite the extensive theoretical and experimental studies that have investigated the stress of external tendons, the proposed expressions are typically complex and differ substantially with regard to how the main parameters are considered [48]. In this section, the relation between the strain of the external tendon ε_p and the mid-span deflection δ is established according to the geometric deformation of a simply supported EPC beam, as shown in Fig. 7.

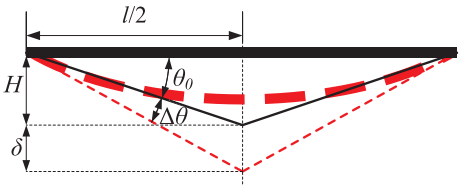

Fig. 7. Geometric deformation relationship.

The lengths of the tendons between the deviators and supports is assumed to be s_1 after the tendons are prestressed, whereas the initial length is s_0. H is the vertical distance between the lower surface of the deviator and the anchor point of the external tendon at the end of the beam. Thus, the strain of the tendons can be calculated as

$$\varepsilon_0 = \frac{s_1 - s_0}{s_0} = \frac{\sqrt{\left(\frac{l}{2}\right)^2 + H^2} - s_0}{s_0} \tag{13}$$

The deviators produce a downward deflection δ after the application of external load, and the lengths of the tendons s_1 become s_2; then,

$$\varepsilon_p = \frac{s_2 - s_0}{s_0} = \frac{\sqrt{\left(\frac{l}{2}\right)^2 + (H + \delta)^2} - s_0}{s_0} \tag{14}$$

The relationship between the strain of the tendons ε_p and the mid-span deflection δ can be described by combining Eqs. (13) and (14) as follows:

$$\varepsilon_p = \sqrt{\frac{l^2 + 4(H + \delta)^2}{l^2 + 4H^2}}(\varepsilon_0 + 1) - 1 \tag{15}$$

Here, the deflection δ is positive when it is downward and negative when it is upward. The force of the prestressing tendon P can then be obtained according to the beam deflection, that is $P(\delta)$.

2.3.4. Resistance model considering strain-rate effects

The dynamic equivalent resistance to blast loadings of the simply supported EPC beam could be calculated using the derived equations presented above in conjunction with the relation between the deflection and strain of materials, as follows:

$$R(\delta, \dot{\varepsilon}) = \frac{M(\varphi, \dot{\varepsilon})}{Bl^2/8} + \frac{F(\delta, \dot{\varepsilon_p})}{Bl/4} \tag{16}$$

where M depends on the curvature φ and strain rate $\dot{\varepsilon}$ of concrete and conventional steel bars, and B is the width of the beam. The dynamic resistance $R(\delta, \dot{\varepsilon})$ is the ability of beams to resist bending deformation under blast loadings, which can be calculated with the uniform static load corresponding to the deformation δ, and taking into account the strain-rate effects $\dot{\varepsilon}$ simultaneously [32].

In this case, the dynamic resistance $R(\delta, \dot{\varepsilon})$ actually includes the contribution of a vertical restoring force $F(\delta, \dot{\varepsilon_p})$, where the direction is opposite to the direction of the external blast loading. Actually, $F(\delta, \dot{\varepsilon_p})$ is a nonlinear function with respect to the mid-span deflection δ and the strain rate of the prestressing steel tendon $\dot{\varepsilon_p}$. However, the strain-rate effect of the external prestressing tendon is not significant because of the low elastic modulus, and it was therefore neglected in this analysis.

A_{ys} and E_{ys} are assumed to be the area and modulus of elasticity of the prestressing tendons, respectively. After the tendons are prestressed, the initial strain of the externally prestressed tendons is $\varepsilon_{y0} = \frac{P_0}{E_{ys}A_{ys}}$. Taking the equilibrium position of the initial anti-deflection

of the beam as the origin, when the downward mid-span displacement δ is generated, according to the developed Eq. (15), the concentrated vertical restoring force can be described as

$$F(\delta) = 2P(\delta)\sin\theta = 2E_{ys}A_{ys}[(\varepsilon_{y0}+1)\sqrt{\frac{l^2+4(H+\delta)^2}{l^2+4H^2}} - 1] \cdot \frac{2(H+\delta)}{\sqrt{l^2+4(H+\delta)^2}} \quad (17)$$

3. Theoretical approach to dynamic responses of EPC beam

3.1. Equation of motion under blast loading

The purpose of the dynamic analysis is to obtain the time-dependent dynamic deflection and stress of the structures, which serves as the basis for the structural design. The equivalent single-degree-of freedom (SDOF) method enables one to convert typical continuous structural systems to SDOF systems and derive their dynamic response parameters [32], which is sufficiently precise [52,53] and is typically used for practical analysis of structures subjected to blast loadings. This approach is taken here because it is precise dynamic analysis is difficult for distributed mass systems, which have an infinite number of degrees of freedom. The equation of motion can be written as follows:

$$M_e\ddot{\delta} + R_e(\delta, \dot{\varepsilon}) = P_e(t) \quad (18)$$

where M_e denotes the equivalent mass, $M_e = K_M M$, K_M denotes equivalent mass factor, which equals 0.5 in the elastic phase and 0.33 in the plastic phase [32], M refers to the beam mass; $P_e(t)$ refers to the equivalent external dynamic load, $P_e(t) = K_L P(t) l$, K_L denotes the equivalent load factor, which equals 0.64 in the elastic phase and 0.5 in the plastic phase, $P(t)$ refers to the uniformly distributed blast load; $R_e(\delta, \dot{\varepsilon})$ denotes the equivalent dynamic resistance, $R_e(\delta, \dot{\varepsilon}) = K_R R(\delta, \dot{\varepsilon})$, K_R represents the equivalent resistance factor, which equals K_L, $R(\delta, \dot{\varepsilon})$ denotes the dynamic resistance. No damping effect has been considered in this study, since it demonstrates no significant effect on the maximum response of structures subjected to blast loadings, and also that it is generally safe to ignore the effect of damping in protective structures [32,38,54]. The explicit algorithm is employed to solve transient problems under blast loadings, where the convergence is conditional and the calculation time step is very small.

3.2. Solutions to equation of motion

The nonlinear equation of motion (Eq. (18)) is solved numerically using the explicit predictor-corrector Newmark algorithm [55,56]. This algorithm establishes predicted values for the displacement, velocity, and acceleration in each time step and then adjusts the predicted values using the corresponding R-δ curve. This method is highly efficient for blast analysis because the equilibrium iteration is avoided in each time step. The detailed steps for solving the algorithm are provided in Refs. [43] and [22].

However, because of the presence of a nonlinear restoring force $F(\delta)$, the calculation of the residual stress in the Newmark algorithm must be corrected as follows.

(a). The estimated value of the reaction force of the external tendons and the external moment are calculated by the estimated value of the deflection δ and then multiplied by the equivalent coefficient of the load to obtain the estimated value of the equivalent restoring force $F_e(\delta)$.
(b). When the residual stress Ψ is calculated, $F_e(\delta)$ is added to the calculation formula, yielding

$$\Psi = f_{n+1} - F_e(\delta) - p(\widetilde{d}_{n+1}, \widetilde{v}_{n+1}) \quad (19)$$

Ψ is divided by the stiffness, and the deflection correction value is obtained to determine the real deflection value of the step.

(c). From the real deflection value, obtaining the true restoring force $F_e(\delta)$ yields the real dynamic resistance.

The computational steps are detailed as follows.

(1) Obtain the initial parameters, including the mid-span deflection δ_0, curvature φ_0, and strain at the middle axis of the cross-section $\bar{\varepsilon}$ based on the layered section method.
(2) Calculate the predictors of displacement, velocity, and acceleration at step n, and then determine the predictor of the cross-section curvature using the δ-ε_u-ε_b relation.
(3) According to the predictor of deflection δ and the layered section method, determine the predictors of the restoring force $F(\delta)$ and the axial compressive force, which is perpendicular to the cross-section.
(4) Combine the rate-sensitive material model and improved layered section method to obtain the predictors of the mid-span moment and dynamic resistance from the predictors of the cross-section curvature and axial compressive force.
(5) Calculate the residual stress from Eq. (19), and then obtain the displacement correction by dividing the residual stress by the equivalent stiffness.
(6) Add the estimated displacement and the correction value to obtain the true value of the deflection at step n.
(7) Calculate the true value of curvature and restoring force and axial compressive force from the true value of deflection.
(8) Calculate the true value of the sectional moment and the dynamic resistance from the real value of the axial compressive force and the curvature according to the layered section method and rate-sensitive material model.
(9) Calculate the real value of velocity and acceleration at step n.
(10) Repeat steps (2)–(9) until the end of the loop is reached or the EPC beam is broken.

4. Verification of the theoretical approach

To verify the accuracy of the proposed theoretical approach, we selected two EPC beams subjected to static loads by Ni et al. [57], and two partially prestressed beams subjected to blast loadings by Cheng et al. [31], as well as numerical simulations of the EPC beams tested in [57] under different blast loadings, conducted in the FE software ABAQUS.

4.1. Verification of the approach for static loads

When the proposed dynamic theoretical approach of the EPC beam is applied to a static analysis, the proposed approach can be verified by existing static load test data without considering the effects of strain rate on the material behavior. This section presents the experimental and numerical analyses of the tested beam specimens PB-3 and PB-4 [57]. The detailed configuration of beam PB-3 is shown in Fig. 8.

The four-point multistage bending loading was adopted during the experiment, and the interval between each loading stage measured approximately 5 min. The corresponding load position is depicted in Fig. 8. The load during each stage measured 15 kN prior to occurrence of cracks within the beam, and the same was reduced to 10 kN post cracking. The loading was stopped when concrete within in the compression zone of the test beam was crushed or the loading system reading no longer demonstrated a rise. At this time, plastic hinges appeared at the beam midspan, and the bearing capacity of the beam was lost.

An FE model of the PB-3 beam was established using the ABAQUS package in accordance with the assumptions listed in section 2.3 by employing 4-node plane stress elements CPS4R for concrete and two-

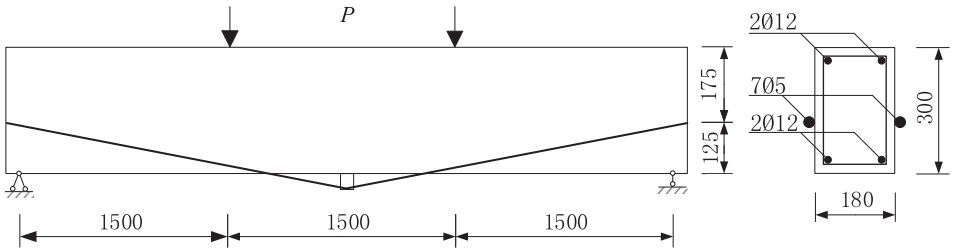

Fig. 8. Configuration of test beam PB-3.

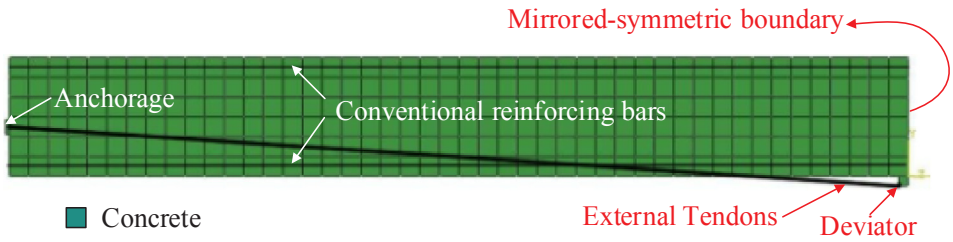

Fig. 9. FE model for PB-3 beam.

dimensional (2-D) truss elements T2S2 for tendons and steel bars [37,58]. An element size of 5 × 5 cm was used in accordance with a mesh sensitivity analysis as well as recommendations from Mercan et al. [59]. Given the symmetry of the PB-3 beam, only one-half of the beam was modelled, as depicted in Fig. 9. Simple support conditions simulating hinge and roller supports were applied to the ends of the beam, and symmetry boundary was applied at the mid-span. The prestressing tendon was embedded into the deviator and anchorage. The interactions between prestressing tendon and deviator, between prestressing tendon and anchorage were modeled by tie constraint in ABAQUS, which considers a node on one surface to be tied to a corresponding node located on the contact surface. The two tied nodes demonstrated identical displacements. The said condition assumes slippage between the two contact surfaces to be negligible. Conventional steel bars were embedded within the beam whilst assuming no slip between steel bars and surrounding concrete.

The damaged plasticity concrete model, which represents a continuum, plasticity-based, damage model in ABAQUS and can be defined to be sensitive to the strain rate under dynamic loading, was considered in this study to be representative of concrete. The steel reinforcement was simulated using the Mises model. Material properties of the deviator and anchorage were considered identical to those of conventional steel bars.

A two-step loading pattern was considered during FE analysis. The first step only accounts for response of the beam when subjected to an effective prestressed force. The second step involves application of actual loads on the beam. The equivalent load method and cooling method are two kinds of prestressing simulation methods [60]. The equivalent load method involves prestress conversion into an equivalent load applied to the structure. The method, however, is based on simplified assumptions, which cannot simulate the spatial prestressed effect on structures. Cooling method is relatively simple and can simulate stress losses, which can be used to simulate prestressing. Considering nonlinear geometric effects, the analysis step was based on the use of the “static general” algorithm.

The ultimate strength of the prestressing steel tendons is $f_u = 1.08 \times 10^3$ MPa, and the concrete tensile and compressive strength are $f_t = 3.0$ MPa and $f_c = 40.77$ MPa, respectively, with a modulus of elasticity of $E_c = 3.25 \times 10^4$ MPa. The yield stresses of Φ12 and Φ16 conventional steel bars are 340 MPa and 380 MPa, respectively. In test beam PB-4, the conventional tensile steel bars are 2Φ16 and 2Φ12 with a corresponding reinforcement area of 628 mm^2, which is different from the 2Φ16 steel bars with a corresponding reinforcement area of 402 mm^2 in beam PB-3. In addition, in PB-4, the initial stress of the prestressing tendons is 667 MPa, which is different from the initial stress of 797 MPa in PB-3. The other parameters are the same as those

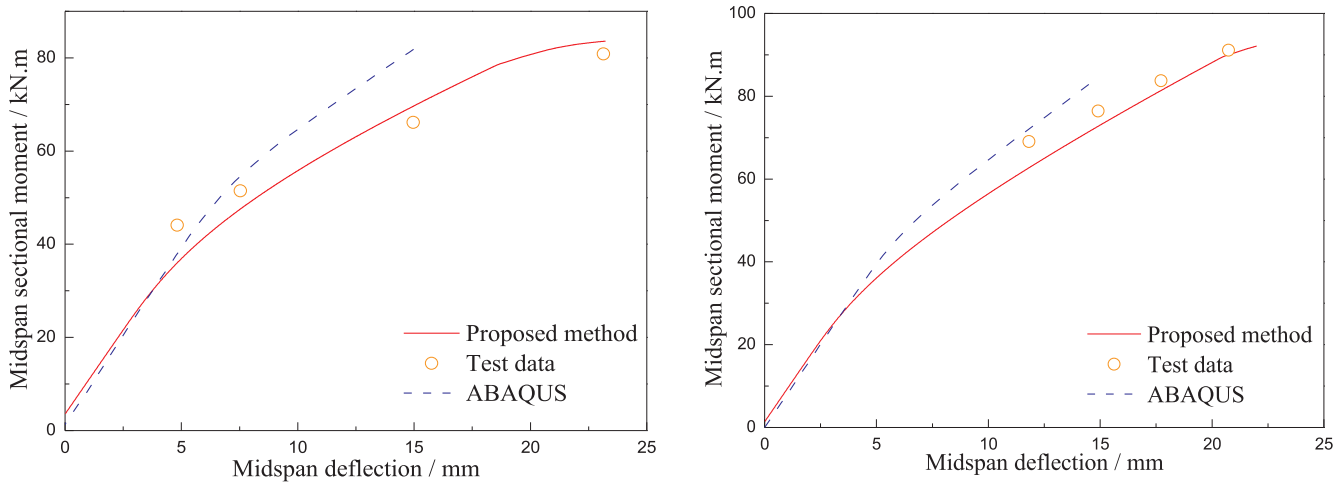

Fig. 10. Moment-deflection curves at mid-span of the test EPC teams.

for both beams.

Fig. 10 shows the mid-span moment-deflection curves of the PB-3 and PB-4 test beams predicted by the proposed dynamic approach and numerical model, illustrating general agreement between the proposed dynamic approach and the experimental and FE data. However, the FE result yields a slightly larger moment after reaching the non-elastic period, and maximum mid-span deflections are smaller, the FE result are considered to be "harder", that is, it appeared as if the bending stiffness of the FE beam had increased. Occurrence of this phenomenon could be possibly attributed to the Poisson ratio of the damaged plasticity model for concrete within ABAQUS, which tends to remain constant during calculations [61]. However, during actual loading, the Poisson ratio of a material is not fixed. Especially when the strain is large, the Poisson ratio increases with the increase of the strain [62], consequently, FE results have been referred to as being "harder".

4.2. Verification of the approach for blast loadings

4.2.1. Based on test data

No experimental study of EPC beams subjected to blast loadings was found in the existing literature. In order to verify the accuracy of the proposed dynamic approach, the test data of two blast-loaded partially prestressed RC beams PC-1 and PC-2 [31] were chosen for analysis, as shown in Figs. 11 and 12. The proposed approach was also degenerated to calculate responses of partially prestressed RC beams subjected to blast loadings. Owing to changes in the arrangement of prestressed tendons, the process to determine the relationship between the sectional moment and curvature was modified when the approach was degenerated with other contents remaining unchanged. Details concerning changes made within process can be found in [22].

The lengths and overall depths of the test beams were 2.6 m and 0.16 m, respectively, and the widths of PC-1 and PC-2 were 0.22 m and 0.24 m, respectively. The other parameters of the test beams PC-1 and PC-2 are listed in Table 1. As depicted in Fig. 11, ends of the two test beams were placed on two walls measuring 0.2 m thick with the inner distance of the walls measuring 2.4 m. Upper surfaces of the beams were covered with a 0.3 m thick soil layer, and a detonating cord was evenly placed above the soil at a distance of 0.45 m away from the soil surface. A soil-pressure transducer and a strain gauge and a displacement transducer were, respectively, installed on the upper and lower surfaces of the beams at an intermediate position, as shown in Fig. 12. Experimental measurements demonstrated the blast load on the beam surface to be uniform. Detailed description of the tests could be found in [31] and [22]. The damage caused to the beams is depicted in Fig. 12 with plastic hinges appearing at the midspan. Moreover, the two beams have been renamed to facilitate ease of description.

The concrete's elastic modulus and cube compressive strength measured at an age of 28 days were 21.3 GPa and 32.4 MPa, respectively. The elastic modulus and corresponding hardening modulus of a conventional steel bar are $E_s = 210$ GPa and $E_{sp} = 18.6$ GPa, respectively. Those for a prestressed steel tendon are $E_p = 199$ GPa and $E_{pu} = 82.4$ GPa, respectively. The yield stress and corresponding yield strain of a conventional steel bar are $f_s = 0.235$ GPa and $\varepsilon_s = 1.12 \times 10^{-3}$, respectively. Those for a prestressed steel tendon are $f_y = 1.49$ GPa and $\varepsilon_y = 7.5 \times 10^{-3}$. The ultimate stress and corresponding ultimate strain of the prestressed steel tendon are $f_{pu} = 1.86$ GPa and $\varepsilon_{pu} = 11.9 \times 10^{-3}$, respectively. The initial prestress was 1116 MPa. The three parameters used in the rate-sensitive model are listed in Table 2.

The simplified blast overpressure curve applied to the beams in the test is shown in Fig. 13, wherein the peak pressure equaled 0.38 MPa. The approximate curve was obtained by simplifying the actual pressure curve and preserving the the peak pressure, total impulse, and time characteristics.

Fig. 14 compares the displacement time histories at mid-span between the predicted results and the test data, and an excellent agreement can be observed here as well. The deflection of PC-2 increased rapidly and the beam was destroyed before the end of the blast loading, which is attributed to the fact that the prestressing tendon ratio of PC-1 was half that of PC-2.

4.2.2. Based on numerical simulation

Based on the FE model established in section 4.1, the blast loading was incorporated into the ABAQUS using the explicit algorithm. However, during the process of simulating prestresses, the rate of cooling must be slow, since rapid cooling tends to form a dynamic load acting on the beam, which in turn, causes beam vibrations and affects calculation results [63,64].

The parameters of the EPC beams for the numerical simulation under blast loadings were the same as those of PB-3. The rising time (tr) and duration (td) of the equivalent triangular loading pulse on PB-3 were 2 ms and 30 ms, respectively, and the peak values of the triangular pulses were 0.1, 0.2, and 0.3 MPa, respectively, as shown in Fig. 15.

Fig. 16 shows the displacement time histories at mid-span of the test beam subjected to blast loadings predicted by the proposed approach and numerical model, which can be seen to agree well with one another. The shapes of the deflection-time curves and maximum mid-span deflections are similar to each other. The maximum mid-span deflections and corresponding times increase with the peak overpressure. However, compared to results obtained using the proposed approach, the observed drop in curves representing simulation results is rather steep. This implies that the beam reaches the peak quickly and rebounds faster. The simulation result, therefore, is "harder", and with increase in blast load, this phenomenon become all-the-more obvious. Probable reason for this phenomenon is that the Poisson ratio is assumed constant during numerical calculations, similar to the case mentioned in Section 4.1. Another reason is that there still is limited error on evaluating the damage accumulation by the damaged plasticity model for concrete in ABAQUS.

Fig. 17 shows the maximum deformation of the EPC beam under blast loadings with different peak overpressures; the shape of the beam is mostly straight, except for a certain area across the mid-span. This result also supports the assumption that the plastic deformation of the beam is mainly concentrated in a certain range of span, referred to as

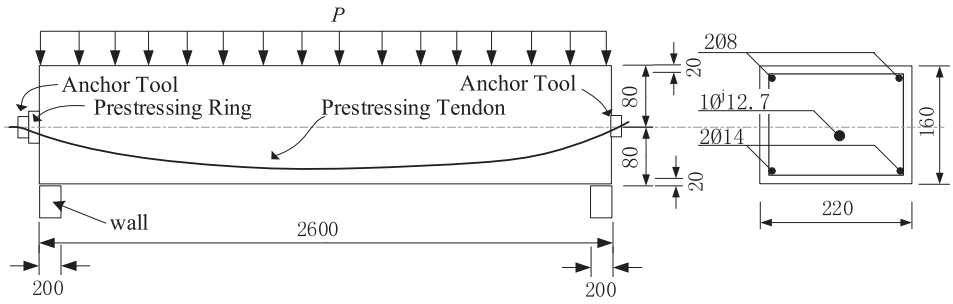

Fig. 11. Configuration of PC-1 test beam [31].

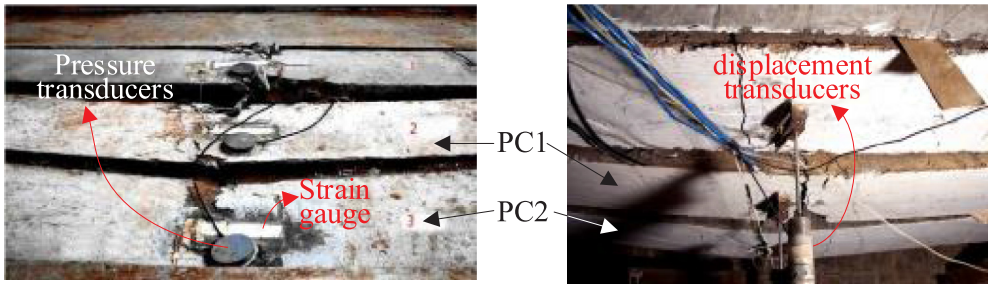

Fig. 12. Failure modes of test specimens [31]. (a) upper surface (b) lower surface.

Table 1
Parameters of test beams.

Specimen	Conventional tensile steel	Prestressing steel	External tendon ratio
PC-1	2Φ14	1Φj12.7	0.35%
PC-2	2Φ12 + 2Φ10	1Φj9.53	0.175%

Table 2
Parameters of the rate-sensitive model.

Material		S (MPa)	N	$\dot{\varepsilon}_*$(/s)
Steel		6	1	0.00005
Concrete	Compression	2.993	2	0.000666
	tension	0.462	2	0.00015

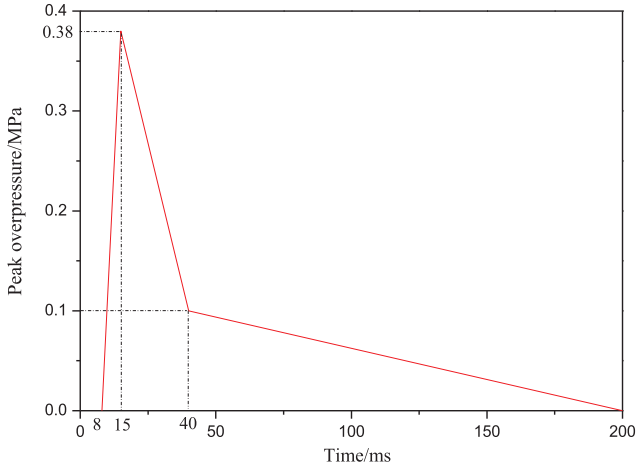

Fig. 13. Simplified blast loading on the test beams.

the plastic hinge in Section 2.3.2.

5. Parameter discussion

Blast-resistant properties of the beam structure actually depend on the resistance function, including the maximum resistance and plastic deformation. This section discusses the influence of three parameters, the conventional reinforcement ratio ρ_s, the prestressing reinforcement ratio ρ_p, and the span-depth ratio l/h, on the proposed theoretical approach's predictions of the dynamic response of the EPC beam subjected to blast loadings, using the EPC beam PB-3 as an example. The rate-sensitive parameters used are same as those listed in Table 2. The peak pressure, rising time (tr), and duration (td) of the triangular blast loading applied to PB-3 are 0.4 MPa, 2 ms, and 30 ms, respectively.

Obviously, the derivation of the proposed theoretical approach is based on the assumption that the response of the beam is flexural only

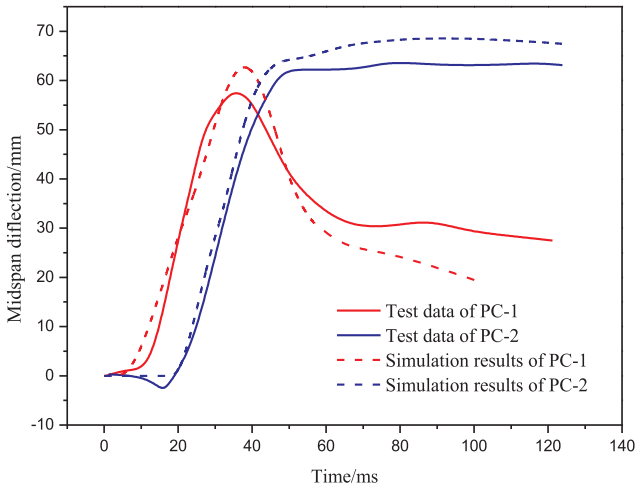

Fig. 14. Mid-span displacement time histories.

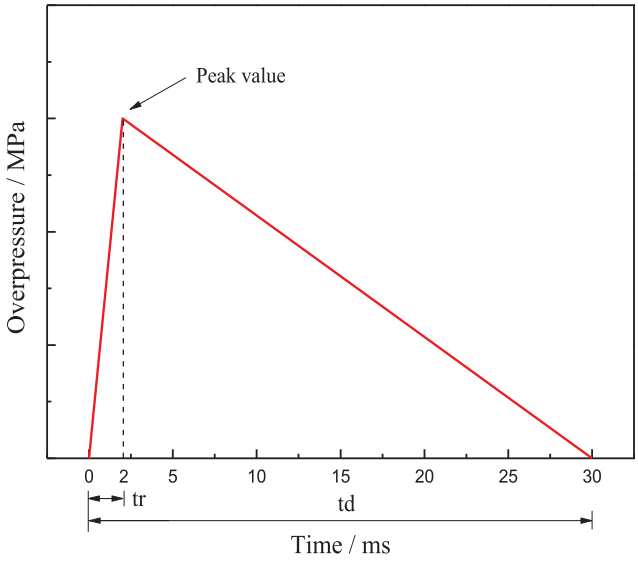

Fig. 15. Simplified triangular blast loading on the test beams.

or flexural governed. In addition, if the rising time and duration of the blast loading is longer than the vibration period, the beam is prone to bending damage.

5.1. Conventional reinforcement ratio (ρ_s)

The displacement time histories at mid-span of the EPC beam with different conventional reinforcement ratios (ρ_s = 0–2.5%) are shown in Fig. 18(a). The EPC beam is symmetrically reinforced by conventional

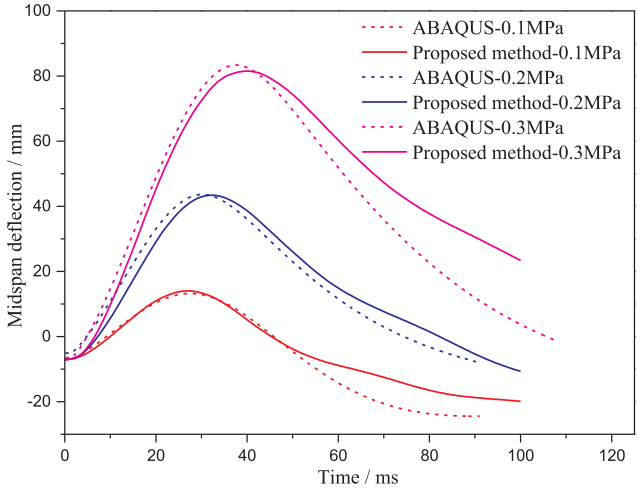

Fig. 16. Mid-span displacement time histories for PB-3.

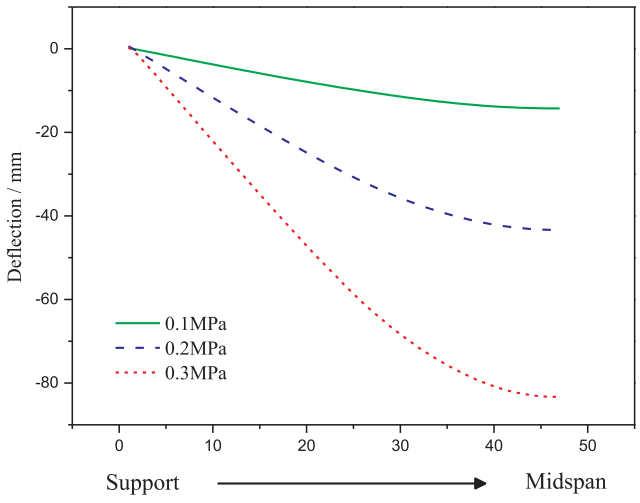

Fig. 17. Maximum deformation of PB-3.

reinforcing bars, and the other parameters are the same as those for PB-3. Fig. 18(a) illustrates that the maximum deflection and the time to reach the maximum deflection decrease with increasing ρ_s. In the case of ρ_s = 0%, the deflection of the beam increases rapidly, and the beam is destroyed before the end of the blast loading. When ρ_s reaches 2%, the effect of the increase in the reinforcement ratio on the decrease in the maximum deflection is no longer obvious. The bending rigidity of the beam increases with increasing ρ_s, which leads to an increase in the vibration frequency of the beam. This result is supported by the displacement time histories at mid-span: when ρ_s reaches 2.5%, the time history exhibits two distinct peaks over the duration of the load.

Fig. 18(b) shows the predicted dynamic resistance time histories of the EPC beam. As shown in this Fig., the maximum dynamic resistance increases with increasing ρ_s. When ρ_s reaches 2.5%, the curve shows two peaks over the duration of the load, which is similar to the mid-span displacement time curve of ρ_s = 2.5%.

Fig. 18(c) shows the curves of dynamic resistance versus deflection, each of which can be divided into four segments: OA, AB, BC, and CO. The dynamic resistance increases rapidly with increasing deflection in segment OA, which is a straight line. In this segment, the beam is still in the elastic deformation stage. However, the dynamic resistance remains unchanged when the deflection increases rapidly in segment AB, which has a similar shape to that of the static load-deflection curve of the externally prestressed specimen, which had a single pair of draped tendons and was tested by Harajli [2]. In this segment, the beam is in

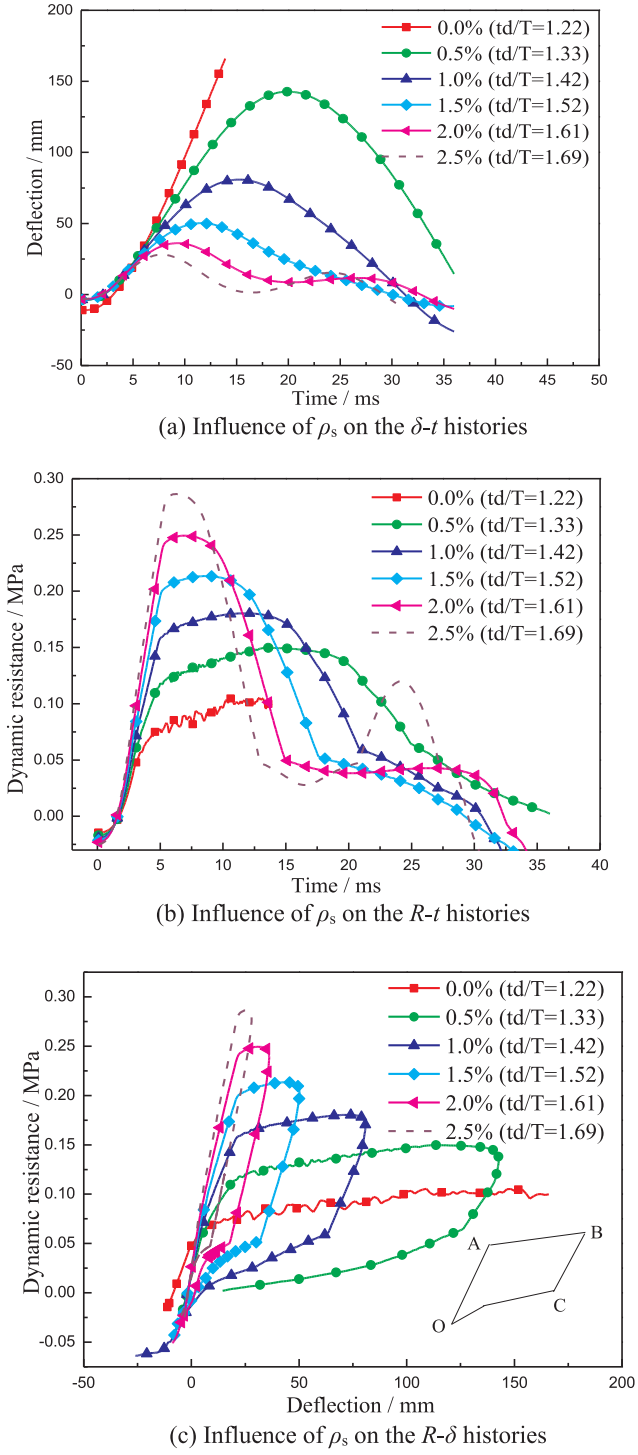

Fig. 18. Influence of conventional reinforcement ratio (ρ_s). (a) Influence of ρ_s on the δ-t histories. (b) Influence of ρ_s on the R-t histories. (c) Influence of ρ_s on the R-δ histories.

the plastic deformation stage. Then, a rebound action appears at inflexion B. Fig. 18(c) illustrates that the size of the elastic deformation is nearly identical to the reduction of ρ_s, whereas the size of the plastic deformation increases significantly. In the case of ρ_s = 0%, the beam is destroyed rapidly. When ρ_s reaches 2.5%, the size of the plastic deformation is approximately zero, which is uneconomical and not expected, particularly in protective structures, although a high value of ρ_s might significantly enhance the dynamic resistance. Therefore, the appropriate configuration of the conventional reinforcement can

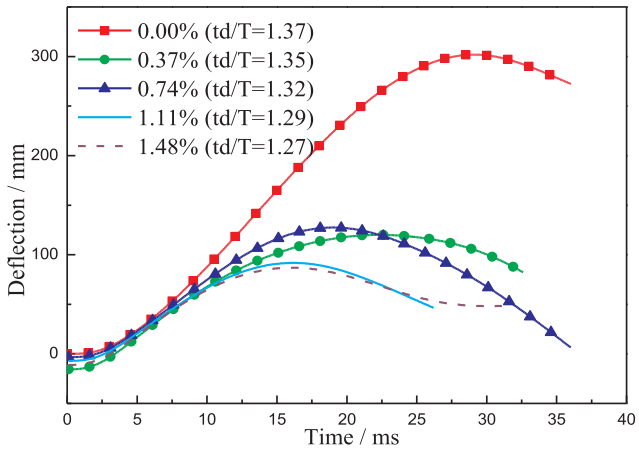

(a) Influence of ρ_p on the δ-t histories

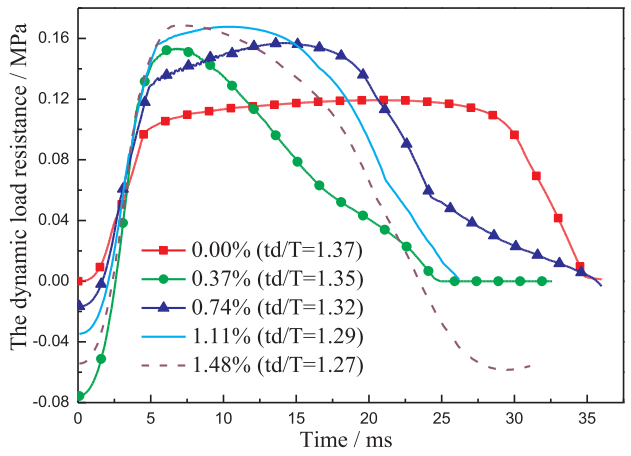

(b) Influence of ρ_p on the R-t histories

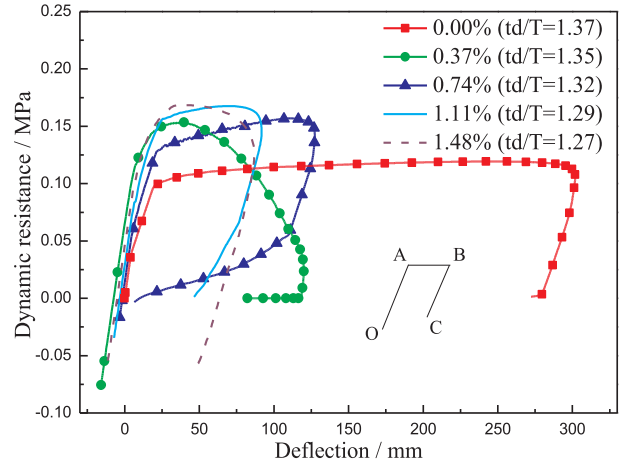

(c) Influence of ρ_p on the R-δ histories

Fig. 19. The influence of prestressing reinforcement ratio (ρ_p). (a) Influence of ρ_p on the δ-t histories. (b) Influence of ρ_p on the R-t histories. (c) Influence of ρ_p on the R-δ histories.

maximize the blast-resistant properties of the EPC beam after the maximum permissible deflection is confirmed.

5.2. Prestressing reinforcement ratio (ρ_p)

The mid-span displacement time curves with different prestressing reinforcement ratios (ρ_p = 0–1.48%) are shown in Fig. 19(a), with the other parameters being the same as those for PB-3 with a ρ_p of 1.02%. Fig. 19(a) illustrates that the maximum deflection and the time required to reach the maximum deflection decrease with increasing ρ_p, which is same as the influence of ρ_p. The beam will be destroyed within a short period with no prestressing reinforcement, and the maximum deflection reaches nearly 300 mm. When ρ_p reaches 1.11%, increases in ρ_p have only a slight effect on the maximum deflection. Fig. 19(b) illustrates that the dynamic resistance increases with increasing ρ_p, although the maximum dynamic resistance of the beam remains largely unchanged after ρ_p reaches 1.11%.

Fig. 19(c) shows the dynamic resistance-deflection curves, each of which can be divided into three segments: OA, AB, and BC. The general properties of segments OA and OB are similar to those in Fig. 18(c). In the case of ρ_p = 0%, the beam is destroyed and can no longer bear a load because of the extent of plastic deformation, from which the beam cannot recover. Fig. 19(c) also illustrates that the maximum dynamic resistance increases with increasing ρ_p; however, when ρ_p reaches 0.74%, the effect of increases in ρ_p on the increase in the maximum dynamic resistance is no longer obvious, although the maximum deflection decreases. Therefore, the dynamic resistance of PB-3 (ρ_p = 1.02%) cannot increase efficiently unless the structural parameters of the beam are changed, such as by increasing the conventional reinforcement ratio.

5.3. Span-depth ratio (l/h)

The mid-span displacement time histories and dynamic resistance time histories with different span-depth ratios (l/h = 6.67–16.7) are shown in Fig. 20(a) and (b), respectively, with the other parameters being the same as for PB-3, which has an l/h of 15. Fig. 20(a) and (b) illustrate that higher values of l/h are associated with more deformation and a lower dynamic resistance, which is similar to the trend in the static case. The beam is essentially in the elastic deformation stage when l/h is 10.0 and 6.67, and thus, the blast-resistant properties of the test beam cannot be used sufficiently, as is also illustrated in Fig. 20(c). In addition, the greater the l/h, the smaller the td/T, the vibration period of the beam with l/h of 6.67 is smaller than the beam with l/h of 10, as shown in Fig. 20(b). More information about the vibration performance of EPC beams could be found in the references introduced in Section 1. In the case of l/h = 16.7, the maximum mid-span deformation is nearly 200 mm. Hence, the value of l/h should be carefully controlled in the design of protective structures.

6. Conclusions

This paper presents a theoretical approach to predict the dynamic responses of EPC beams subjected to uniformly distributed blast loadings that have a single pair of draped tendons, combining a rate-sensitive material model with an improved layered section method. The new theoretical approach was developed under the framework of a SDOF system, and computational steps are summarized and listed. The proposed approach is only appropriate to the case when the response of the beam is flexural governed. Based on the research studies presented herein, the following conclusions are drawn.

(1) The explicit predictor-corrector Newmark algorithm is improved by the proposed approach. When the residual stress is calculated, the influence of the deviator on the beam is considered, and the calculation precision and efficiency are improved.
(2) Numerical and theoretical results demonstrated that a plastic hinge would appear in the mid-span of a simply supported EPC beam with a deviator subjected to blast loadings, which is similar to that under the static loads. The influence of the length of the plastic hinge is considered in the theoretical approach.
(3) A corresponding calculation program was compiled on the MATLAB

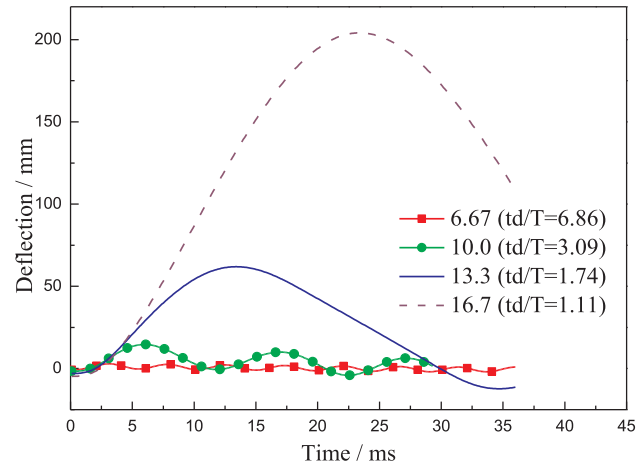

(a) Influence of l/h on the δ-t histories

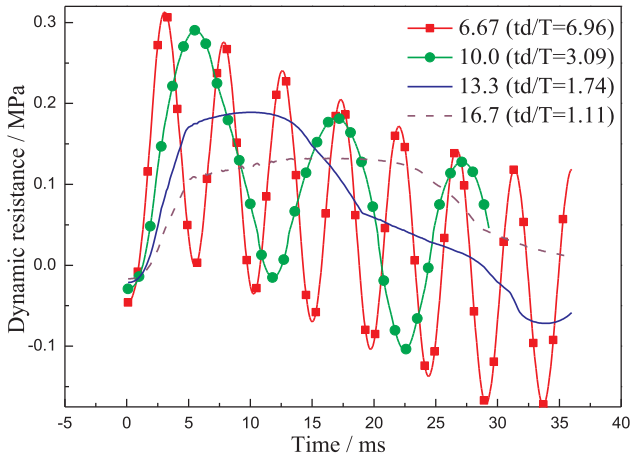

(b) Influence of l/h on the R-t histories

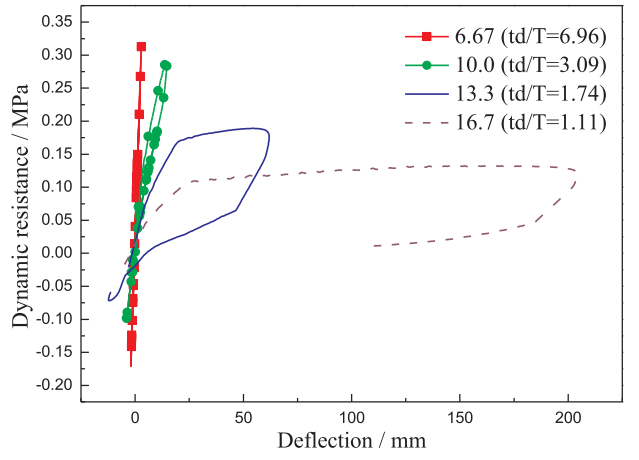

(c) Influence of l/h on the R-δ histories

Fig. 20. The influence of span-depth ratio (l/h). (a) Influence of l/h on the δ-t histories. (b) Influence of l/h on the R-t histories. (c) Influence of l/h on the R-δ histories.

platform. Testing beams subjected to static loadings and blast loadings, as well as a developed FE model, were employed to verify the effectiveness of the proposed approach and compiled program, and the analytical results predicted by the proposed approach agreed well with the experimental data.

(4) The effects of three arrangement parameters (the conventional reinforcement ratio ρ_s, prestressing reinforcement ratio ρ_p and span-depth ratio l/h) were analyzed. The dynamic resistance increased with increasing ρ_s and ρ_p and with decreasing l/h, but the increase was finite. Therefore, the values of the three arrangement parameters should be balanced to take full advantage of the blast-resistant capacity of the EPC beams.

Acknowledgements

This work was supported by the National Basic Research Program of China [grant numbers 2016YFC0305200, 2015CB058003]; and the National Natural Science Foundation of China [grant number 51622812]. We would like to thank Editage [www.editage.cn] for English language editing.

References

[1] Atta AM, Khalil EH. Strengthening of RC beams with opening in shear zone using external prestressing technique. Mag Concrete Res 2015;67:133–44.
[2] Harajli MH. Strengthening of concrete beams by external prestressing. PCI J 1993;38:76–88.
[3] Dall'Asta A, Dezi L. Nonlinear behavior of externally prestressed composite beams: analytical model. J Struct Eng 1998;124:588–97.
[4] Harmanci YE, Michels J, Czaderski C, Motavalli M. Calculation technique for externally unbonded cfrp strips in structural concrete retrofitting. J Eng Mech 2016;142(6):04016026.
[5] Lou T, Lopes SMR, Lopes AV. Numerical modeling of externally prestressed steel-concrete composite beams. J Constr Steel Res 2016;121:229–36.
[6] Wang X, Shi J, Wu G, Yang L, Wu Z. Effectiveness of basalt FRP tendons for strengthening of RC beams through the external prestressing technique. Eng Struct 2015;101:34–44.
[7] Zhai C, Chen L, Xiang H, Fang Q. Experimental and numerical investigation into RC beams subjected to blast after exposure to fire. Int. J. Impact Eng 2016;97:29–45.
[8] Aparicio AC, Ramos G, Casas JR. Testing of externally prestressed concrete beams. Eng Struct 2002;24:73–84.
[9] Lou TJ, Lopes AV, Lopes SMR. Influence of span-depth ratio on behavior of externally prestressed concrete beams. ACI Struct J 2012;109:687–95.
[10] El-Ariss B. Stiffness of reinforced concrete beams with external tendons. Eng Struct J Earthquake Wind Ocean Eng 2004;26:2047–51.
[11] Ghallab A, Beeby AW. Factors affecting the external prestressing stress in externally strengthened prestressed concrete beams. Cem Concr Compos 2005;27:945–57.
[12] Cao Q, Jiang H, Wei R, Deng Y. Shear behavior of anchor blocks in externally prestressed concrete bridges. Struct Build 2016;169:657–68.
[13] Ghallab A. Calculating ultimate tendon stress in externally prestressed continuous concrete beams using simplified formulas. Eng Struct 2013;46:417–30.
[14] Pisani MA. Behaviour under long-term loading of externally prestressed concrete beams. Eng Struct 2018;160:24–33.
[15] Qi J, Wang J, Ma ZJ, Tong T. Shear behavior of externally prestressed concrete beams with draped tendons. ACI Struct J 2016;113:677–88.
[16] El-Shafiey T, Atta A. Retrofitting of reinforced concrete beams in shear using external prestressing technique. Mag Concrete Res 2012;64:201–11.
[17] Wang J, Qi J, Zhang J. Optimization method and experimental study on the shear strength of externally prestressed concrete beams. Adv Struct Eng 2014;17:607–16.
[18] Song T, Shen Y, Li G. Moment redistribution in EPC continuous curved box beams. J Bridge Eng 2017;22(8):04017035.
[19] Lou T, Lopes SMR, Lopes AV. Effect of linear transformation on nonlinear behavior of continuous prestressed beams with external FRP cables. Eng Struct 2017;147:410–24.
[20] Grace NF, Abdelsayed G. Behavior of externally draped CFRP tendons in prestressed concrete bridges. PCI J 1998;43:88–101.
[21] Ghallab A. Ductility of externally prestressed continuous concrete beams. KSCE J Civ Eng 2014;18:595–606.
[22] Chen L, Fang Q, Liu JC, Zhang YD, Xiang HB. Nonlinear analysis of blast performance of partially prestressed RC beams. Int J Protect Struct 2011;2:295–314.
[23] Chen W, Hao H, Chen S. Numerical analysis of prestressed reinforced concrete beam subjected to blast loading. Mater Des 2015;65:662–74.
[24] Ngo T, Mendis P, Krauthammer T. Behavior of ultrahigh-strength prestressed concrete panels subjected to blast loading. J Struct Eng 2007;133:1582–90.
[25] Cramsey N, Naito C. Analytical assessment of the blast resistance of precast, prestressed concrete components. PCI J 2007;52:67–80.
[26] Cofer WF, Matthews DS, Mclean DI. Effects of blast loading on prestressed girder bridges. Shock Vib 2015;19:1–18.
[27] Park YH, Park C, Park YG. The behavior of an in-service plate girder bridge strengthened with external prestressing tendons. Eng Struct 2005;27:379–86.
[28] Chen J, Zhang M, Liu W. Vibration serviceability performance of an externally prestressed concrete floor during daily use and under controlled human activities. J Perform Construct Fac 2015;30(2):04015007.
[29] Miyamoto A, Tei K, Nakamura H, Bull JW. Behavior of prestressed beam strengthened with external tendons. J Struct Eng 2000;126:1033–44.
[30] Shi L, He H, Yan W. Prestress force identification for externally prestressed concrete

beam based on frequency equation and measured frequencies. Math Probl Eng 2014;2014:1–13.
[31] Cheng SY, Yan DJ, Zhai JM, Li YZ, Cai QH, Xu GX. Experimental comparative study on pc beams dynamic performance with different adhering form prepress. Appl Mech Mater 2013;256–259:991–4.
[32] Krauthammer T. Modern protective structures. Boca Raton, FL: CRC Press; 2008.
[33] Lou TJ, Xiang YQ. Finite element modeling of concrete beams prestressed with external tendons. Eng Struct 2006;28:1919–26.
[34] Izzuddin BA, Fang Q. Rate-sensitive analysis of framed structures part I: model formulation and verification. Struct Eng Mech 1997;5:221–37.
[35] Sima JF, Roca P, Molins C. Cyclic constitutive model for concrete. Eng Struct 2008;30:695–706.
[36] Jacinto AC, Ambrosini RD, Danesi RF. Experimental and computational analysis of plates under air blast loading. Int J Impact Eng 2001;25:927–47.
[37] Chen L, Fang Q, Zhang Y, Zhang Y. Rate-sensitive numerical analysis of dynamic responses of arched blast doors subjected to blast loading. Trans Tianjin U 2008;14:348–52.
[38] Station UA. TM5-855-1 Fundamentals of protective design for conventional weapons. US Army, Navy and Air Force, US Government Printing Office, Washington DC; 1986.
[39] Fang Q, Izzuddin BA. Rate-sensitive analysis of framed structures part II: Implementation and application to steel and R/C frames. Struct Eng Mech 1997;5:239–56.
[40] Malvern LE. The propagation of longitudinal waves of plastic deformation in a bar of material exhibiting a strain-rate effect. J Appl Mech 1951;18:203–8.
[41] Perzyna P. Fundamental problems in viscoplasticity. Adv Appl Mech 1966;9:243–377.
[42] Wu C, Oehlers DJ, Day I. Layered blast capacity analysis of FRP retrofitted RC member. Adv Struct Eng 2009;12:435–49.
[43] Pan L, Chen L, Fang Q, Zhai CC, Pan T. A modified layered-section method for responses of fire-damaged reinforced concrete beams under static and blast loads. Int J Protect Struct 2016;7(4):495–517.
[44] Tan KH, Ng CK. Effect of deviators and tendon configuration on behavior of externally prestressed beams. ACI Struct J 1997;94:13–22.
[45] Senthil R, Manisekar R. Ultimate flexural behaviour of externally prestressed new beams and distressed beams. Carbon 2015;10:461–84.
[46] Manisekar R, Senthil R. Stress at ultimate in unbonded post tensioning tendons for simply supported beams: a state-of-the-art review. Adv Struct Eng 2006;9:321–35.
[47] Harajli MH, Mabsout ME, Al-Hajj JA. Response of externally post-tensioned continuous members. ACI Struct J 2002;99:671–80.
[48] Harajli MH. On the stress in unbonded tendons at ultimate: critical assessment and proposed changes. ACI Struct J 2006;103:803–12.
[49] Corley WG. Rotational capacity of reinforced concrete beams. J Struct Div 1966;92:121–46.
[50] Yang C, Zhu F, Zheng W. The research of plastic hinge of unbonded prestressed concrete beams. Low Temp Architect Technol 2005;5:53–4. (in chinese).
[51] Park R, Paulay T. Reinforced concrete structures. John Wiley & Sons; 1975.
[52] Morison CM. Dynamic response of walls and slabs by single-degree-of-freedom analysis—a critical review and revision. Int J Impact Eng 2006;32:1214–47.
[53] Henrych J, Abrahamson GR. The dynamics of explosion and its use. J Appl Mech 1979;47:218.
[54] Clough RW, Penzien J, Griffin DS. Dynamics of structures. J Appl Mech 2013;44:366.
[55] Newmark NM. A method of computation for structural dynamics. J Eng Mech Div 1959;85:67–94.
[56] Owen DR, Hinton E. Finite elements in plasticity. Pineridge Press; 1980.
[57] Ni W, Zhang Y, Qin Y. Calculation approach for deflection of external prestressed concrete beam. J Civ Eng Manage 2004;21:75–7. (in Chinese).
[58] Genikomsou AS, Polak MA. Finite element analysis of punching shear of concrete slabs using damaged plasticity model in ABAQUS. Eng Struct 2015;98:38–48.
[59] Mercan B, Schultz AE, Stolarski HK. Finite element modeling of prestressed concrete spandrel beams. Eng Struct 2010;32:2804–13.
[60] Wang C, Shen Y, Yang R, Wen Z. Ductility and ultimate capacity of prestressed steel reinforced concrete beams. Math Probl Eng 2017;2017:1–6.
[61] Hong J, Fang Q, Chen L, Kong X. Numerical predictions of concrete slabs under contact explosion by modified K&C material model. Constr Build Mater 2017;155:1013–24.
[62] Kupfer HB. Behavior of concrete under biaxial stresses. J Eng Mech Div 1969;99:853–66.
[63] Hibbitt HD, Karlsson BI, Sorensen EP. ABAQUS-EPGEN: a general-purpose finite element code; 1983: 3.
[64] Chen L, Fang Q, Guo Z, Liu J. An improved analytical method for restrained RC structures subjected to static and dynamic loads. Int J Struct Stab Dy 2014;14:304–1150.